WWW.IJRPR.COM

International Journal of Research Publication and Reviews

Journal homepage: www.ijrpr.com ISSN 2582-7421

Preparation and Characterization of Bimetallic-Epoxy Conducting Nanocomposites

Muhammad Ishtiaq Husain [a], Dr. Muhammad Sultan[*b], Muhammad Rafique [c], Mahmood ul Hassan Khan [d]

[a, b] Department of Physical Sciences, UET Taxila, Pakistan
[c,d] Department of Chemistry, Quaid e Azam University, Islamabad
muhammadrafiquepk@g.mail.com, mahmoodchem@gmail.com

ABSTRACT

$NiMn_2O_4$ nanoparticles were successfully fabricated in the presence of natural compounds such as carboxymethylcellulose (CMC). The use of CMC polymer as a capping agent and a protecting agent during the nanoparticle's formation was crucial to the synthesis of $NiMn_2O_4$ nanoparticles. Electron microscopy (SEM), energy dispersion spectroscopy (EDS), ultraviolet-visible spectroscopy, and X-ray diffraction (XRD) were used to characterize the synthesized $NiMn_2O_4$ nanoparticles. The present sample's single-phase cubic structure was validated by XRD measurements, and the lattice parameter was discovered to be 8.3131Å. Additionally, the XRD data demonstrate good crystallinity, with an average crystallite size of 27.18 nm. After the optical characteristics of the anticipated samples were inspected using UV–vis diffuse reflectance spectroscopy, the bandgap of the sample was estimated to be approximately 1.7 eV. After the Electrical conductivity tests using the four-probe technique of the final sample, it is observed that the sample of concentration ratio 2:8 has shown maximum AC Conductance reaching $3.5x10^{-7}$ as frequency increases up to $2x10^6$. The sample of concentration ratio 3:7 has shown maximum AC Conductance reaching $1.5x10^{-7}$ as frequency increases up to $2x10^6$. In continuation, the sample of concentration ratio 4:6 has shown maximum AC Conductance reaching $2.5x10^{-8}$ as frequency increases up to $2x10^6$. The findings will contribute to the advancement of Nano composite materials, paving the way for their utilization in fields such as electronics, aerospace, and energy storage.

1. Introduction

The study of nanotechnology has grown in popularity in recent years. The foundation of nanotechnology is nanoparticles. With a size of less than 100 nm, nanoparticles are exceedingly small particles that can contain metal, carbon, metal oxides, or organic materials [1]. In contrast to their larger-sized siblings, the nanoparticles exhibit distinctive physiochemical and biological properties. This impact can be credited to various factors such as increased mechanical strength, higher surface area in relation to volume, or increased chemical stability. Nanoparticles have an extensive variety of appliances because of their unique characteristics. In addition to their material differences, nanoparticles vary in size, shape, and dimension [2]. For many years, noble metal nanoparticles have been created and investigated. These materials have proven to be helpful in a variety of applications, such as imaging, nanomedicine, and both homogeneous and heterogeneous catalysis [3]. Highly sophisticated synthesis techniques have been used, allowing for specific control over the morphology and size of the particles [4]. Although they were discovered later, bimetallic nanoparticles are currently a fascinating field of study since they provide a new level of flexibility in terms of modifying the properties of the particle by combining two metals into one. This increases their suitability for use in biomedicine, imaging, and catalysis (including electrocatalysis) [5, 6].

Nanoparticle characteristics are directly impacted by synthesis methods. Magnetic properties are influenced by changes in the inherent distribution of trivalent and divalent cations between these two locations as well as by changes in the size, circulation, and shape of crystallite particles [7, 8]. There are numerous physical and chemical methods for creating nanocrystalline substances. The processes of co-precipitation, hydrothermal reactions, sol-gel, non-chemical breakdown, and thermal degradation using chemical procedures or organic precursors are frequently employed. Simple oxides have recently been chemically generated by short-term, low-temperature reactions between inorganic salts and gelatin. One simple tactic among these that is becoming more and more popular is the organic intermediates approach [9-11].

Utilizing natural materials as surfactants to produce nanocrystalline inorganic compounds is an alternative synthesis method. Examples of these materials include mineral oil and carboxymethylcellulose (CMC). This paper reports on the co-precipitation method that we utilized, together with CMC solution as a surfactant, to synthesize $NiMn_2O_4$ nanoparticles. An important factor to take into account while choosing CMC is that it is a biodegradable, non-toxic, and nutritive material. The resulting compounds were subjected to morphological and structural characterization [12, 13]. The fabrication of BNPs is an important field of research and appliances with various possible applications and increased tensile strength, hardness, and toughness are just a few

of the mechanical properties that bimetallic epoxy nanocomposites can exhibit. This performance is useful for the construction and aerospace sectors [14]. In comparison to conventional epoxy resins, these nanocomposites have better temperature stability. Because of this feature, BNPs can be used in high-temperature settings such as coatings and electronics. Additionally, certain BNPs can have their electrical conductivity qualities modified for usage in applications like as antistatic coatings and electromagnetic shielding [15, 16].

The metals in the nanocomposite may or may not show catalytic activity, depending on their selection. This can be utilized for a variety of catalytic processes, such as chemical synthesis or environmental cleanup. It is possible to design bimetallic epoxy nanocomposites with effective corrosion resistance. This is useful in sectors like the maritime and oil and gas industries where corrosion protection is essential [17]. Bimetallic epoxy nanocomposites can aid in the production of lightweight materials, lowering energy consumption in transportation and increasing fuel economy, thanks to their improved characteristics. By using bimetallic nanocomposites, materials that are more resilient and long-lasting may be developed, possibly lowering the need for regular replacements or repairs. This may help cut down on waste and the use of resources [18].

The fields of materials science and nanotechnology benefit from research on bimetallic epoxy nanocomposites. Our knowledge of interactions at the nanoscale and the possible uses of nanomaterials is increased. Numerous industries use these nanocomposites, including electronics, aerospace, automotive, construction, and even biomedical devices [19]. Because of these materials' adaptability, developments in their synthesis may have far-reaching effects. The development of novel materials with better qualities has the potential to boost the economy by expanding markets, generating employment, and possibly lowering manufacturing costs across a range of industries. By lowering the need for frequent replacements or enabling more energy-efficient solutions in production and transportation, bimetallic epoxy nanocomposites can be engineered to increase environmental sustainability [20, 21].

Research on bimetallic epoxy nanocomposites can uncover unexpected phenomena and features with broad significance for materials science and nanotechnology and contribute to our understanding of materials at the nanoscale.

2. Materials and methods

Figure 1: Synthesis of $NiMn_2O_4$ nanoparticles by Co-precipitation method.

The reagents used are $NiCl_2 \cdot 6H_2O$, $MnCl_2 \cdot 2H_2O$, NaOH, and carboxymethylcellulose (CMC) 1% solution. For thirty minutes, the aqueous solutions of 0.4 $MnCl_2 \cdot 6H_2O$ and 0.2 M $NiCl_2 \cdot 6H_2O$ were incorporated and stirred. An aqueous solution of 3 M NaOH was added after CMC, a capping agent, was incorporated to the mixture. The pH of the mixture was regularly checked and kept between 11 and 12. For 60 minutes, the solution was continuously agitated while being heated to 80°C and then the mixture was permitted to cool to room temperature. Using ethanol and water, a blackish precipitate was isolated and repeatedly cleaned. After 12 hours at 110°C, the precipitate turned black. The samples were heated to 800°C for a period of six hours in the furnace.

3. Results and Discussion

The X-ray diffraction (XRD), UV-Vis (ultraviolet spectroscopy), energy-dispersive X-ray spectroscopy (EDX), and scanning electron microscopy (SEM) are frequently used techniques for characterizing materials. XRD is utilized to find the phase composition and crystal structure of the material, while SEM-EDX provides information about the surface morphology and elemental composition. UV-Vis spectroscopy is used to explore the optical characteristics of the material, like band gap energy and absorbance characteristics. The combined results of these analyses offer a comprehensive understanding of the structural, elemental, and optical characteristics of the material, which is essential for various scientific and technological applications.

3.1 X-ray diffraction (XRD) Analysis:

The $NiMn_2O_4$ nanoparticles were fabricated, and their crystallinity, phase purity, and structure were confirmed utilizing powder X-ray diffraction patterns. Figure 2. indicates the XRD pattern of synthesized $NiMn_2O_4$ and the primary peak linked with planes (111), (220), (311), (222), (400), (511), and (440) which are accurately matched with the standard $NiMn_2O_4$ with the JCPDS card Number 00 − 001 − 1110 signifying the cubic structure with space group F. Furthermore, this pattern of XRD demonstrates that $NiMn_2O_4$ nanoparticles do not exhibit primary formation of peaks. The following formula is used to calculate the lattice constant which is derived from the XRD peak positions. The results are shown in Table 1.

$$a = \frac{\lambda\sqrt{h^2+k^2+l^2}}{2\sin\theta}$$

Where hkl denotes the miller indices of each plane in the XRD pattern, θ represents Bragg's angle, and λ shows the wavelength of the X-ray beam applied.

The following formula is used to compute the X-ray density of synthesized $NiMn_2O_4$ nanoparticles, and the results are displayed in Table 1.

$$\rho_x = \frac{ZM_w}{V_{cell}\,N_A}$$

Where Z is the formula unit present in the unit cell, M_w is the molecular weight of the fabricated NPs and N_A is Avogadro's number.

$Vcell = a^3$

From the following formula, we have calculated the crystallite size of synthesized $NiMn_2O_4$ nanoparticles.

$$D = \frac{k\lambda}{\beta cos\theta}$$

Where λ is the X-ray beam wavelength, k is Scherrer's constant, β is the full-width half maximum of the peak and the average crystallite size of the synthesized NPs is demonstrated in Table 1

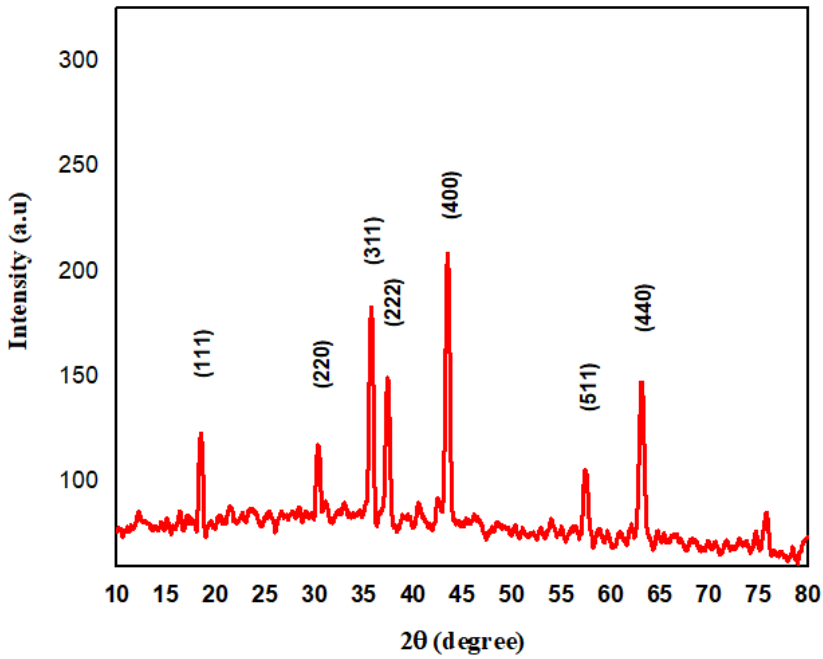

Figure 2: XRD diffraction of Ni-Mn_2O_4

Table 1: Experimental lattice constants (a_{exp}), the volume of the unit cell (V or a3), the crystallite size (nm), and the density of X-ray (g cm-3), structural data determined from XRD data for Ni-Mn_2O_4 nanoparticles.

S. No.	Sample	Lattice constant (a=b=c) (Å)	Volume(V) ($Å^3$)	Crystallite Size (nm)	X-ray density ρ_x (gcm^{-3})
1	Ni-Mn_2O_4	8.3141	574.706	27.18	5.322

3.2. Scanning Electron Microscope Analysis

The histogram chart depicted in Figure 3 displays particle size distribution and the surface morphology of the fabricated $NiMn_2O_4$ NPs, as find by the use of ImageJ software. The chunk-shaped nanoparticles with varying sizes were observed in the current sample. Since the total interface energy keeps decreasing and there is no discernible morphology in Figure 3, some agglomeration is also seen in the produced nanoparticles due to magnetic dipolar couplings and Vander Wall forces between synthesized NPs. As seen in Figure 4, the 40 nanoparticles were taken into account while calculating the average particle size of the NPs using the ImageJ software.

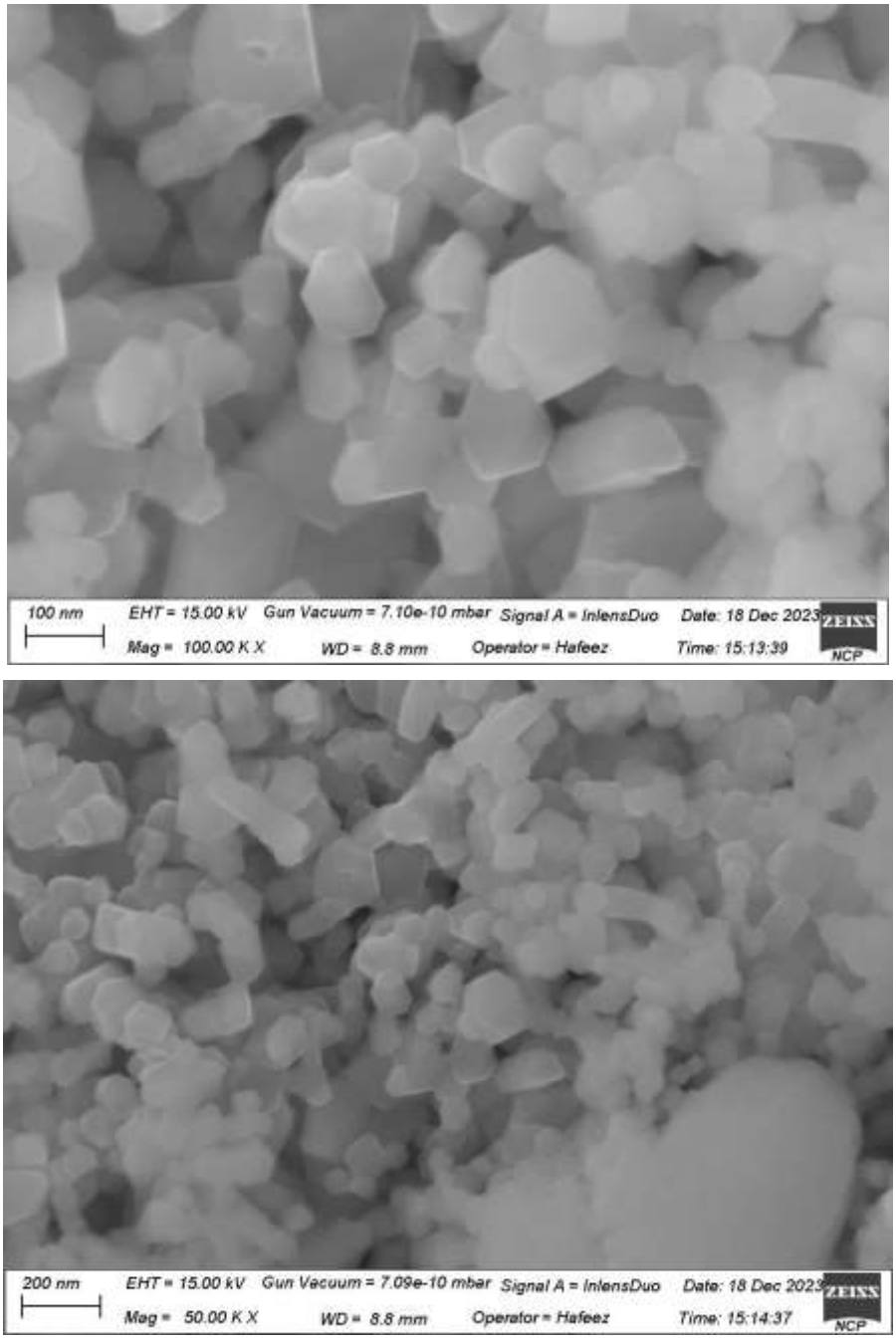

Figure 3: SEM images of $NiMn_2O_4$ nanoparticles

Additionally, the results of the SEM and the crystallite size estimated from the XRD study shown in Table 1 agree rather well.

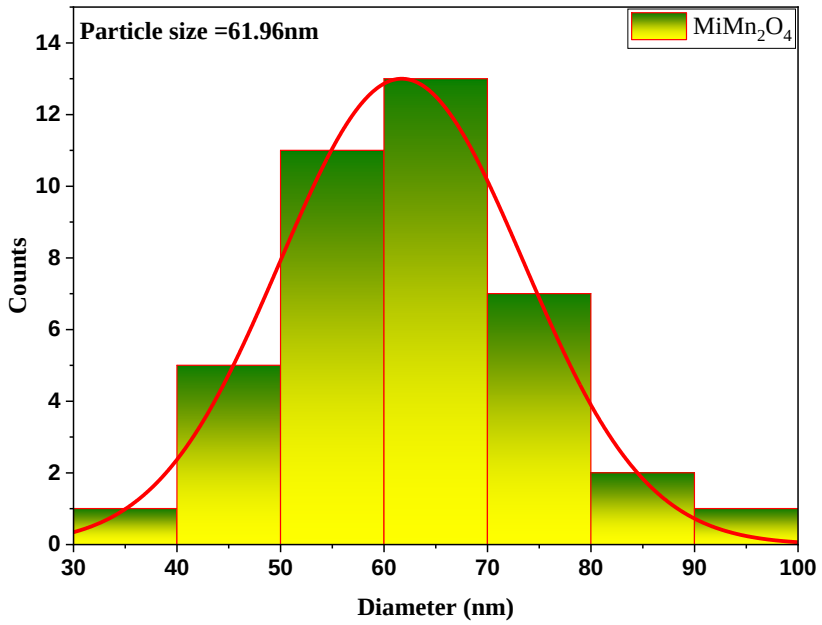

Figure 4: Histogram of the particle size distribution of $NiMn_2O_4$ NPs

3.3. Energy dispersion Spectrum (EDS):

The EDS spectrum is used to find the composition of elements of fabricated $NiMn_2O_4$ NPs. EDS investigation was used to confirm the existence of Ni, Mn, Ca, and O, and their proportion is displayed in Figure 5. Using EDS analysis, the existence of the $NiMn_2O_4$ nanoparticle phase and the precise elemental weights were verified. This indicates that the synthesis of $NiMn_2O_4$ nanoparticles can be significantly enhanced by the co-precipitation approach. We employed carboxymethylcellulose (CMC) during the manufacture of the samples, hence some Ca peaks were also seen in the EDX spectrum. The samples were sprayed with carbon (C) to improve the validity of their morphology before SEM analysis. This explains why, when doing the Energy Dispersion Spectrum (EDS) study, some small peaks of C were also noticed

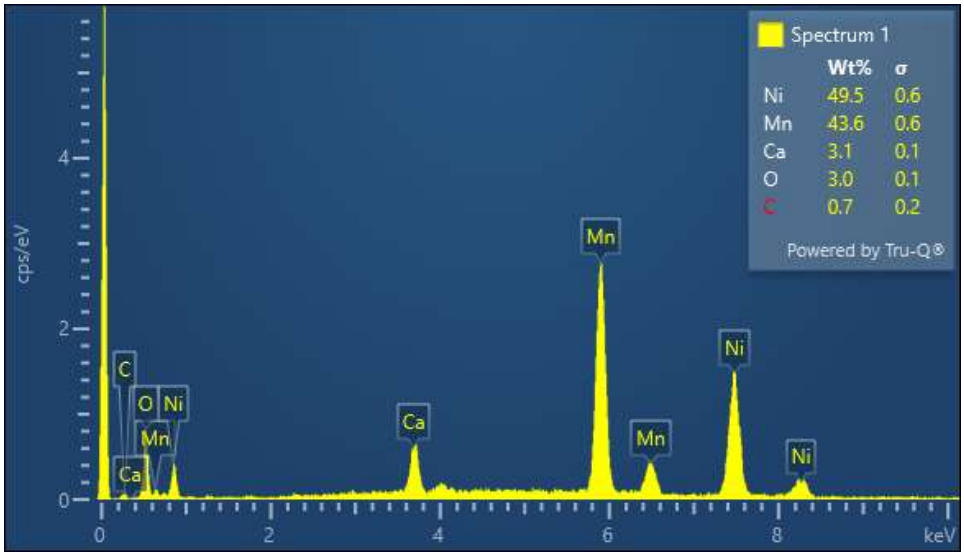

Figure 5: EDX spectral analysis for the elemental composition of $NiMn_2O_4$ NPs.

3.4. Ultraviolet-visible (UV-Vis) spectroscopy:

At room temperature (RT), $NiMn_2O_4$ nanoparticles were analyzed using a UV-visible diffused reflectance spectrum. Because there are fewer scattering effects, the UV-Vis DRS provides than the wavelength of the incoming light. The direct bandgap for the $NiMn_2O_4$ nanoparticles system was discovered in this work, with an estimated Eg = 1.7eV as shown in the Figure.

It is well known that one of the most important aspects in making use of photocatalytic applications is the bandgap of nanostructured materials. Figure 5 illustrates the $NiMn_2O_4$ nanoparticles' diffuse reflectance spectroscopy. The sample bandgap was determined using the subsequent formula

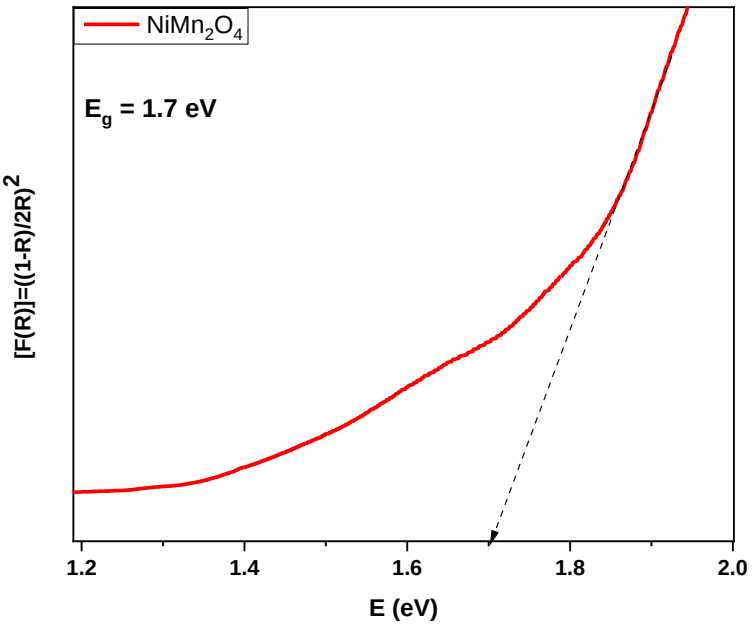

Figure 6: UV-visible diffused reflectance spectra showing variation of [FR× h (ν)]2 as a function of hν for $NiMn_2O_4$ NPs

UV-visible diffuse reflectance spectroscopy, shown in Figure 6, is one of the most significant techniques to identify the optical properties of the synthesized nanoparticles. This method is based on the Kubelk-Munk function.

For each wavelength, Rα represents the reflectance of an infinitely thick sample used as a reference. The Kubelka–Munk function is the absorption coefficient's analog. The nanomaterial's bandgap energy values were estimated using the slope of the $[F(R\alpha)h\nu]^2$ against hν graph. These plots are given by:

$$\alpha h\nu = A(h\nu - Eg)$$

Where n is a constant that depends on the type of electronic transition, α is the amount of absorbance, A is a constant of the material, hν is the photon energy, and Eg is the material's optical bandgap. The linear section of the plots of the $(\alpha h\nu)^2$ curve was extrapolated in return hν to the energy axis to determine the energy gap (Eg) of the samples. The $NiMn_2O_4$ NPs had a band-gap (Eg) of 1.7eV.

3.5. Electrical conductivity of Nanoparticles dissolved in Epoxy matrix

The following graphs are obtained by the electrical conductivity tests of the final sample, nanoparticles dissolved in an epoxy matrix.

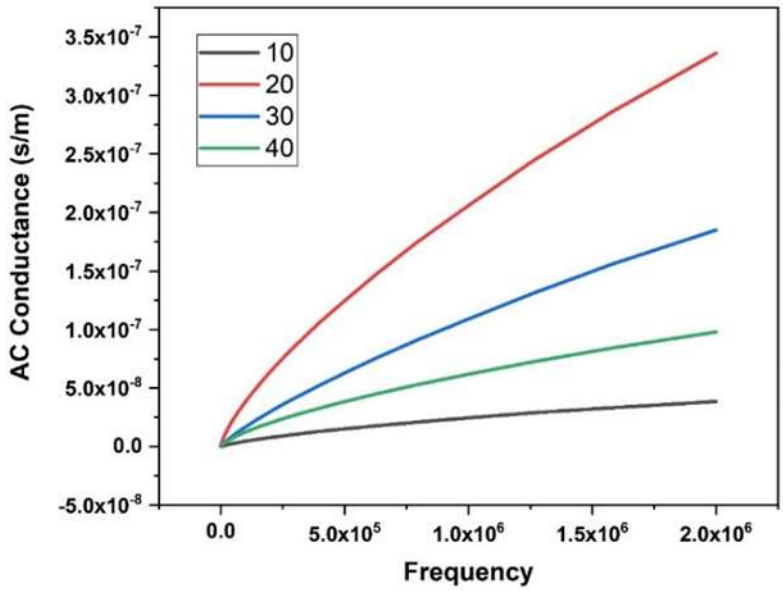

Figure 7: relationship of AC Conductance and frequency

Figure 7 shows the relationship between AC Conductance and frequency of the final sample with the NP-Epoxy ratios 1:9, 2:8, 3:7, and 4:6 respectively.

Figure 7 shows the correlation between frequency and AC conductance for a sample with different ratios of nanoparticles (NP) to epoxy (1:9, 2:8, 3:7, and 4:6). The conductance behavior changes with increasing NP content (from a 1:9 to 4:6), possibly suggesting how the concentration and dispersion of nanoparticles within the epoxy matrix alter the material's electrical properties. We can observe that as frequency rises, the conductance may also rise or fall, depending on the material's frequency-dependent response and the NP-epoxy interaction. For maximizing or minimizing conductance at specific frequencies, the shifting ratios demonstrate how different compositions affect the overall conductivity. When it comes to applications requiring particular frequency responses, Figure 7 is essential for comprehending the electrical performance of these composite materials.

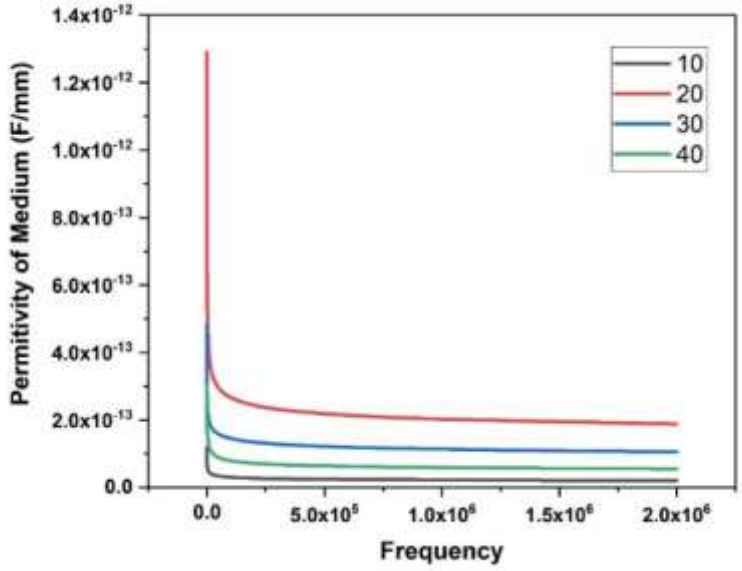

Figure 8: relationship of Permittivity of Medium and frequency

Figure 8 shows the relationship between the Permittivity of the Medium and frequency of the final sample with the NP-Epoxy ratio 1:9, 2:8, 3:7, and 4:6 respectively. For a sample with different nanoparticle (NP) to epoxy ratios—1:9, 2:8, 3:7, and 4:6—Figure 8 shows the link between the medium's permittivity and frequency. As the frequency and NP concentration in the epoxy matrix fluctuate, so does permittivity—a measurement of a material's

ability to influence the electric field inside it. The permittivity behavior may show different trends as the NP content increases (from 1:9 to 4:6), indicating how the interaction between NPs and the epoxy matrix affects the material's electrical energy storage capacity. Permittivity normally declines as frequency rises, but the NP-epoxy ratio determines how much this change occurs. It is crucial to see how the graph illustrates how various compositions impact the composite material's dielectric characteristics.

4. Conclusions

A novel technique for fabricating nanocrystalline $NiMn_2O_4$ has been presented forth, stabilizing discrete nanoparticle structures with carboxylate capping ligands. In this way, the NiMn2O4 nanoparticles were attained with an average diameter of 61.96nm. A stoichiometric combination of transition metal chloride salts in a CMC solution at 500°C, irregular morphologies of $NiMn_2O_4$ nanoparticles have been created via the wet chemical fabrication approach. The annealed samples' XRD diffraction patterns demonstrate the phase purity of the nanocrystalline powders. Lattice parameters were found to be 8.3141 Å. Confirmation of morphological analysis was done by SEM and found the average particle is 61.96nm and the composition of elements was done by EDS investigation. Optical properties were confirmed by the UV-visible diffused reflectance spectrum (DRS) The direct bandgap for $NiMn_2O_4$ nanoparticles system was discovered in this work, with an estimated Eg = 1.7eV.

After the Electrical conductivity tests using four probe technique of the final sample it is observed from the above shown graphs that the sample of concentration ratio 2:8 has shown maximum AC Conductance reaching $3.5x10^{-7}$as frequency increases up to $2x10^{6}$. The sample of concentration ratio 3:7 has shown maximum AC Conductance reaching $1.5x10^{-7}$ as frequency increases up to $2x10^{6}$. In continuation the sample of concentration ratio 4:6 has shown maximum AC Conductance reaching $2.5x10^{-8}$ as frequency increases up to $2x10^{6}$.

5. References

[1] S. Hasan, "A review on nanoparticles: their synthesis and types," Res. J. Recent Sci, vol. 2277, p. 2502, 2015.

[2] Y. Khan et al., "Classification, synthetic, and characterization approaches to nanoparticles, and their applications in various fields of nanotechnology: A review," Catalysts, vol. 12, no. 11, p. 1386, 2022.

[3] G. Bardi, L. Boselli, and P. P. Pompa, "Anti-inflammatory potential of platinum nanozymes: mechanisms and perspectives," Nanoscale, 2023.

[4] M. A. Dheyab et al., "Monodisperse gold nanoparticles: A review on synthesis and their application in modern medicine," International Journal of Molecular Sciences, vol. 23, no. 13, p. 7400, 2022.

[5] D. Zhang, B. Gökce, and S. Barcikowski, "Laser Synthesis and Processing of Colloids: Fundamentals and Applications," Chemical Reviews, vol. 117, no. 5, pp. 3990-4103, 2017/03/08 2017.

[6] E. Ringe, "Nanocrystalline materials: recent advances in crystallographic characterization techniques," IUCrJ, vol. 1, no. 6, pp. 530-539, 2014.

[7] R. Álvarez-Chimal and J. Á. Arenas-Alatorre, "Green synthesis of nanoparticles. A biological approach

" 2023.

[8] N. Li, P. Zhao, and D. Astruc, "Anisotropic gold nanoparticles: synthesis, properties, applications, and toxicity," Angewandte Chemie International Edition, vol. 53, no. 7, pp. 1756-1789, 2014.

[9] S. Kumari et al., "A comprehensive review on various techniques used for synthesizing nanoparticles," Journal of Materials Research Technology Network analysis separation, 2023.

[10] L. Bai et al., "Synthesis of metallic nanocrystals: from noble metals to base metals," Materials, vol. 12, no. 9, p. 1497, 2019.

[11] B. M. Leonard, "Synthesis and characterization of nanocrystalline binary and ternary intermetallic compounds," Texas A & M University, 2010.

[12] F. Sedighi, A. Sobhani-Nasab, M. Behpour, and M. Rahimi-Nasrabadi, "Photocatalytic degradation of rhodamine B, and phenol red dyes using NiMn2O4 nanoparticles prepared by a new approach," Journal of Nanostructures, vol. 9, no. 2, pp. 258-267, 2019.

[13] S. J. Rajoba et al., "Synthesis and electrochemical performance of mesoporous NiMn2O4 nanoparticles as an anode for lithium-ion battery," Journal of Composites Science, vol. 5, no. 3, p. 69, 2021.

[14] A. K. Kushwaha, M. John, M. Misra, and P. L. Menezes, "Nanocrystalline materials: synthesis, characterization, properties, and applications," Crystals, vol. 11, no. 11, p. 1317, 2021.

[15] K. A. Altammar, "A review on nanoparticles: characteristics, synthesis, applications, and challenges," Frontiers in microbiology, vol. 14, p. 1155622, 2023.

[16] N. Baig, I. Kammakakam, and W. Falath, "Nanomaterials: A review of synthesis methods, properties, recent progress, and challenges," Materials advances, vol. 2, no. 6, pp. 1821-1871, 2021.

[17] T. K. Das, M. Jesionek, Y. Çelik, and A. Poater, "Catalytic polymer nanocomposites for environmental remediation of wastewater," Science of the Total Environment, vol. 901, p. 165772, 2023.

[18] İ. Avan, H. Nasirov, İ. Kani, and A. Ozcan, "ZnS/CuS nanocomposites: synthesis and catalytic activity on thymol oxidation," Journal of Sol-Gel Science Technology vol. 107, no. 1, pp. 149-160, 2023.

[19] A. U. Kini, M. Shettar, M. Gowrishankar, and S. Sharma, "A technical review on epoxy-nanoclay nanocomposites: Mechanical, hygrothermal and wear properties," Cogent Engineering, vol. 10, no. 2, p. 2257949, 2023.

[20] A. K. Kushwaha, M. John, M. Misra, and P. Menezes, "Nanocrystalline materials: synthesis, characterization, properties, and applications," Crystals, vol. 11, no. 11, p. 1317, 2021.

[21] L. Bertolacci, P. Valentini, and P. P. Pompa, "A nanocomposite hydrogel with catalytic properties for trace-element detection in real-world samples," Scientific Reports, vol. 10, no. 1, p. 18340, 2020.